IMAGE TAMPERING DETECTION BY EXPOSING BLUR TYPE INCONSISTENCY

Khosro Bahrami and Alex C. Kot

School of Electrical and Electronic Engineering, Nanyang Technological University, Singapore 639798
Email: {khosro1 and eackot}@ntu.edu.sg

ABSTRACT

In this paper, we propose a novel method for image tampering detection in multi-type blurred images. After block-based image partitioning, a space-variant prior for local blur kernels is proposed for local blur kernels estimation. Then, the image blocks are clustered using a k-means clustering based on the similarity of local blur kernels to generate blur type invariant regions. Finally, blur types of the regions are classified into out-of-focus or motion blur using a minimum distance classifier. The experimental results show that the proposed method successfully detects and classifies the regions blur types which outperforms the state-of-the-art techniques. Our proposed approach is used to detect inconsistency in the partial blur types of an image as an evidence of image tampering.

Index Terms— Tampering detection, image splicing, partial blur type detection.

1. INTRODUCTION AND BACKGROUND

Using photo-editing softwares, image tampering can be done easily and detection of tampered images is difficult by human vision system. Since images can be used in journalism, police investigation and as court evidences, image tampering can be a threat to security of people and human society. Therefore, development of reliable methods for image integrity examination and image tampering detection is important. Image splicing is one of the most common types of image tampering. In image splicing, if the original image and spliced region have different blur types such as motion and out-of-focus, an inconsistency in the blur type may appears in the tampered image. The objective of the current work is image splicing detection by exploration of the inconsistency in the partial blur types. To the best of our knowledge, this is the first work that uses out-of-focus and motion blur type inconsistency for image splicing detection. Fig.1 (a) is an authentic image with motion blur and Fig.1 (b) is a tampered image generated from the image in (a) by splicing. The tampered image has inconsistent blur types in the background and the sign. The background with motion blur indicates movement of camera with respect to the scene, while the sign with out-of-focus blur does not have any clue of motion blur. This blur inconsistency can be used as an evidence of tampering.

(a) (b)

Fig. 1. (a) An authentic image with motion blur (b) A tampered image generated from the image (a) which has inconsistent blur types in the background (motion blur) and the sign (out-of-focus blur).

The existing techniques in the image forensics are divided into two categories, including active and passive [1]. The most important passive techniques can be categorized into (1) pixel-based such as re-sampling [2] and contrast enhancement detection [3]; (2) format-based [4]; (3) camera-based such as demosaicing regularity [5-7], and sensor pattern noise [8]; (4) physically-based such as light anomalies [9]. Each technique has some limitations. For instance, the resampling technique is only applicable to uncompressed images and JPEG with minimal compression [2]. The format-based technique does not work when the same quantization is used in the second compression [4].

Some works [10-14] have been proposed for image tampering detection based on blur degree inconsistency. However, these methods can not detect blur type inconsistency. Kakar *et al.* [15] proposed an method for splicing detection based on inconsistency in the motion blur degree and direction. However, this method is only applicable for motion blur. Some works have been done for blur type detection and classification. Chen *et al.* [16] proposed a method based on lowest directional high-frequency energy to estimate direction and region of motion blur. Liu *et al.* [17] used correlation of shifted blocks to classify motion and out-of-focus blurs. Su *et al.* [18] proposed a technique for segmentation of motion and out-of-focus blurred regions based on alpha channel. Aizenberg *et al.* [19] proposed a technique for classification of motion, gaussian and uniform blurred blocks based on magnitude of cepstrum coefficients. However, for natural blurred blocks, the approach in [19] has not high performance. The limitation

978-1-4799-2893-4/14/$31.00 ©2014 IEEE

of the methods in [16-19] is that they do not have high performance for partial blur type detection. They partition the image into blocks and use a feature to classify the blur type of the blocks. However, in real situations, the blur type of the image blocks is affected by the size of the block, blur degree and content which are not considered in these methods. We move on one step further and propose two-step approach to detect the blur types at block and region levels.

The rest of this paper is organized as follows. In section 2 we propose a method for partial blur type detection and classification used for tampering detection. Results and discussions are shown in section 3. Section 4 concludes the paper.

2. PROPOSED METHOD

The proposed method for image splicing detection is explained in details in the following sections.

2.1. Local Blur Kernels Estimation

Given a color image B of size $M \times N$, we first convert it to the gray scale image G and then partition G into non-overlapping blocks $G_{i,j}$ with $L \times L$ pixels, where i and j are index of blocks ($1 \leq i \leq \lfloor \frac{M}{L} \rfloor$, $1 \leq j \leq \lfloor \frac{N}{L} \rfloor$). For an image block $G_{i,j}$, the image blurring process is represented by

$$G_{i,j} = I_{i,j} * K_{i,j} + N_{i,j} \tag{1}$$

where $I_{i,j}$ is a sharp image block, $K_{i,j}$ is a local blur kernel, $N_{i,j}$ is the image block noise and $*$ denotes convolution.

To estimate $K_{i,j}$ from $G_{i,j}$, the Blind Image Deconvolution (BID) is used which estimate $K_{i,j}$ and $I_{i,j}$ from $G_{i,j}$. Using the method in [20] to solve the BID in a Bayesian framework, a maximum a posteriori (MAP) technique is incorporated to estimate $K_{i,j}$ and $I_{i,j}$. However, appropriate prior model play a key role in optimization problem to solve BID. By choosing more accurate models for $K_{i,j}$ and $I_{i,j}$, better result can be obtained. Also, the blur in the image is space-variant, choosing proper priors for $K_{i,j}$ can be effective in the improvement of the final result. In the literature, the existing methods used sparse or gaussian prior model for the blur kernel [21, 22]. However, in the images with multiple blur types such as motion and out-of-focus, choosing the same prior model for all local blur kernels is not suitable for the task of kernel estimation.

We study on the statistics of motion and out-of-focus blur kernels to find appropriate priors for local blur kernels. We blur 400 sharp images with out-of-focus and motion blur with various specifications and estimate the local blur kernels of the images. Fig. 2 (a-b) and (c-d) plots the pixel value distribution of the out-of-focus and motion blur kernels for various blur degrees, respectively. Motion blur kernels tend to be sparse because most values in the kernel are zeros while out-of-focus blur kernels have less tendency to be sparse. Although the kernel sparseness also depends on the blur degree which means low blur degree kernels are more sparse than high blur degree images, the motion blur kernels have more tendency to be sparse than out-of-focus blur kernels. The distribution of out-of-focus blur kernels are closer to Gaussian while the one for motion blur kernels are closer to hyper-laplacian. Therefore, by choosing a prior model closer to Gaussian for out-of-focus blur kernels and a prior model closer to hyper-laplacian for motion blur kernels, better results can be achieved.

Generalized Gaussian Distribution (GGD) has been used extensively to parameterize natural scene statistic of the images [23]. Since GGD is a parametric family of Gaussian, laplace and hyper-laplacian distributions, we use the GGD as the prior model of the local blur kernels. Therefore, prior model of local blur kernel $K_{i,j}$ is defined using GGD as

$$P(K_{i,j}) = e^{||K_{i,j}||^{\gamma_{i,j}}} \tag{2}$$

where $\gamma_{i,j}$ is the shape-parameter of the distribution [23]. For different $\gamma_{i,j}$ values, the GGD represents different distributions. For instance, $\gamma_{i,j} = 2$ indicates Gaussian, $\gamma_{i,j} = 1$ represents laplacian and $\gamma_{i,j} < 1$ depicts hyper-laplacian.

We calculate $\gamma_{i,j}$ of the blur kernel distributions in Fig. 2. The value of $\gamma_{i,j}$ for out-of-focus blur kernels are (a) 1.3840 and (b) 1.5970 while for motion blur kernels, the $\gamma_{i,j}$ values are (c) 0.5390 and (d) 0.6010. Since the distributions of out-of-focus blur kernels are closer to Gaussian, $1 < \gamma_{i,j} \leq 2$ while for motion blur kernels, $0 < \gamma_{i,j} \leq 1$ to be more sparse.

To indicate the value of $\gamma_{i,j}$ for blur kernel prior model, we propose a method using a set of candidate parametric blur kernels. In the prior work [24], the shock filter is used for enhancement of sharp edges from blurred step edges which has an iterative form as $F_{t+1} = F_t - \text{sign}(\Delta F_t)||\nabla F_t||$, where F_t and F_{t+1} are the image at iterations t and $t+1$, ΔF_t is the Laplacian and ∇F_t is the gradient of F_t. By assuming $F_0 = G_{i,j}$, the sharp version of $G_{i,j}$ denoted as $G^s_{i,j}$ is estimated. We use a set of candidate motion blur kernels $\{K_{m_1}, ..., K_{m_u}\}$ and out-of-focus blur kernels $\{K_{o_1}, ..., K_{o_v}\}$ with different specifications to blur $G^s_{i,j}$, given by

$$G^p_{i,j} = K_p * G^s_{i,j}\ ,\ K_p \in \{K_{m_1}, ..., K_{m_u}, K_{o_1}, ..., K_{o_v}\} \tag{3}$$

Consequently, $G^p_{i,j} \in \{G^{m_1}_{i,j}, ..., G^{m_u}_{i,j}, G^{o_1}_{i,j}, ..., G^{o_v}_{i,j}\}$ is the blurred version of $G^s_{i,j}$ generated by the set of candidate blur kernels. The blurred block $G^p_{i,j}$ with the highest similarity to $G_{i,j}$ indicates the closest candidate blur kernel to the actual blur kernel $K_{i,j}$. To measure the similarity of $G^p_{i,j}$ to $G_{i,j}$, we use L_1 norm distance $d^p_{i,j} = ||G^p_{i,j} - G_{i,j}||_1$. Therefore, $d^{m_1}_{i,j}, ..., d^{m_u}_{i,j}, d^{o_1}_{i,j}, ..., d^{o_v}_{i,j}$ are the similarity distances of $G^{m_1}_{i,j}, ..., G^{m_u}_{i,j}, G^{o_1}_{i,j}, ..., G^{o_v}_{i,j}$ to $G_{i,j}$, respectively. The minimum distance of $d^{m_1}_{i,j}, ..., d^{m_u}_{i,j}$ denoted as $d^{m'}_{i,j}$ and $d^{o_1}_{i,j}, ..., d^{o_v}_{i,j}$ indicated as $d^{o'}_{i,j}$ are used to calculate the probability that $K_{i,j}$ is motion or out-of-focus blur kernel defined

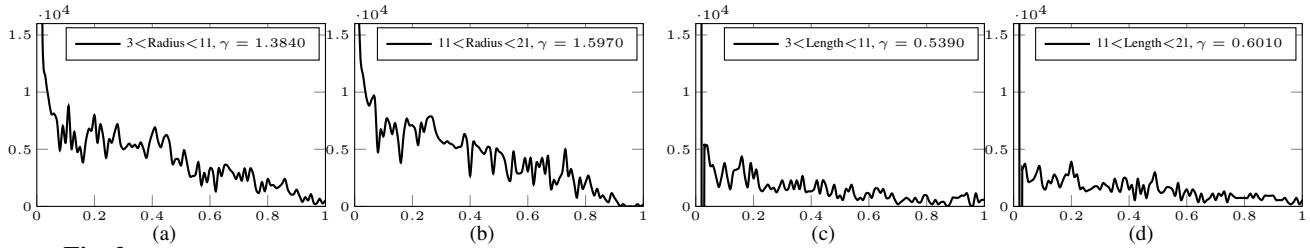

Fig. 2. Pixel value distributions of (a-b) out-of-focus blur kernels and (c-d) motion blur kernels with various specifications.

as

$$P_m(K_{i,j}) = \frac{d_{i,j}^{o'}}{d_{i,j}^{o'} + d_{i,j}^{m'}} \ , \ P_o(K_{i,j}) = \frac{d_{i,j}^{m'}}{d_{i,j}^{o'} + d_{i,j}^{m'}} \quad (4)$$

If $d_{i,j}^{m'} = d_{i,j}^{o'}$, $P_m(K_{i,j}) = P_o(K_{i,j}) = \frac{1}{2}$. If $d_{i,j}^{m'} < d_{i,j}^{o'}$, $0 < P_m(K_{i,j}) < \frac{1}{2} < P_o(K_{i,j}) < 1$ and for $d_{i,j}^{m'} > d_{i,j}^{o'}$, $0 < P_o(K_{i,j}) < \frac{1}{2} < P_m(K_{i,j}) < 1$. Following the study on the shape-parameter, if $P_m(K_{i,j}) > P_o(K_{i,j})$, $0 < \gamma_{i,j} \leq 1$ and for $P_m(K_{i,j}) < P_o(K_{i,j})$, $1 < \gamma_{i,j} \leq 2$. Therefore, we define $\gamma_{i,j}$ for local blur kernels $K_{i,j}$ using $P_o(K_{i,j})$ or $P_m(K_{i,j})$ as

$$\gamma_{i,j} = 2P_o(K_{i,j}) = 2(1 - P_m(K_{i,j})) \quad (5)$$

2.2. Local Blur Kernels Similarity-Based Clustering

For blur kernel estimation, it is usually advantageous to use larger region of the blurred image to increase the accuracy of blur kernel. However, the blur in the region should be invariant in terms of type to achieve better result in blur kernel estimation. In this step, the image blocks with similar blur kernels are clustered together to generate space-invariant blur type regions. We use k-means clustering by incorporating the intensity of local blur kernels pixels and the coordinates of the image blocks in the image as the input features.

Given a set of local blur kernels $K_{1,1}, K_{1,2}, ..., K_{\lfloor \frac{M}{L} \rfloor, \lfloor \frac{N}{L} \rfloor}$ of an image where $M \times N$ and $L \times L$ are the size of image and image blocks, respectively. The feature vector of the clustering is defined as a d-dimensional vector including pixel intensity of the local blur kernels and the coordinates (i, j) of the image blocks. For local blur kernels with size of $\kappa \times \kappa$ and (i, j) as horizontal and vertical coordinates in the image, we define the feature vector $V = [K_{i,j}(1,1), K_{i,j}(1,2), ..., K_{i,j}(\kappa,\kappa), i, j]$ with $d = \kappa \times \kappa + 2$ features as the input. The k-means clustering partitions the image blocks into s regions $R_1, R_2, ..., R_s$ to minimize the within-cluster sum of squares between pixels of kernels where s is the number of clusters.

2.3. Region Blur Type Classification for Image Tampering Detection

After segmentation of the image G into s regions, the image is represented by s layers formation model as $G = \eta_1 \times R_1 + ... + \eta_s \times R_s$, where $R_1, ..., R_s$ are the regions and $\eta_1, ..., \eta_s$ are the binary masks representing the regions. By representation of the image G with s layers model, the image blurring process in Eq. 1 is formulated as $G = \eta_1 \times (I_1 * K_1 + N_1) + ... + \eta_s \times (I_s * K_s + N_s)$, where $K_1, ..., K_s$ are the blur kernels of s regions $R_1, ..., R_s$. To identify the blur type of the regions, a minimum distance classifier is used to measure the normalized cross-correlation proposed in [25] of the estimated blur kernels $K_1, ..., K_s$ and a set of candidate motion blur kernels $\{K_{m_1}, ..., K_{m_u}\}$ and out-of-focus blur kernels $\{K_{o_1}, ..., K_{o_v}\}$ with different specifications. Finally, a human evaluation is needed to detect any inconsistency between the blur type and the image regions. For instance, if a region of the image has hand shake motion blur and another region has out-of-focus, this is an inconsistency in the blur types.

3. RESULTS AND DISCUSSION

In this section, firstly we compare our method with some of the state-of-the-art techniques in partial blur type detection and classification proposed by Chen *et al.* [16], Su *et al* [18] and Aizenberg *et al.* [19]. For the experiments, we define $\{K_{m_1}, ..., K_{m_u}\}$ as the set of candidate motion blur kernels where the length is increased from 2 to 40 pixels and the angle is increased from 0 to 180 degree with the step of 1, and $\{K_{o_1}, ..., K_{o_v}\}$ as the set of out-of-focus blur kernels where the radius is increased from 2 to 40 with the step of 0.1. We set up datasets of blurred images by collecting 400 out-of-focus and motion blurred images from Flicker photo sharing website [26]. The images are partitioned into blocks and the out-of-focus and motion blurred image blocks are manually selected as the ground-truth. We select 2000 blurred blocks (1000 motion and 1000 out-of-focus) with size of 64×64, 1000 blurred blocks (500 motion and 500 out-of-focus) with size of 128×128 and 600 blurred blocks (300 motion and 300 out-of-focus) with size of 256×256.

We compare our method with Chen *et al.* [16], Su *et al.* [18] and Aizenberg *et al.* [19] to classify natural out-of-focus and motion blurred blocks. We define two classes including out-of-focus blur as positive class and motion blur as negative class. Therefore, true positive rate (TPR) is the fraction of out-of-focus blurred blocks that are correctly classified as out-of-focus blur and true negative rate (TNR) is the fraction of motion blurred blocks that are correctly classified as motion blur. Accuracy is defined as the number of correctly classified blocks over the number of all blocks. Table 1 compares the performance of methods. Although, by increasing the block size from 64×64 to 256×256, the accuracy of all methods is

Table 1. Comparison of methods for classification of out-of-focus and motion blurred blocks

Approach	Block Size	TPR (%)	TNR (%)	Type I Error (%)	Type II Error (%)	Accuracy (%)
Chen *et al.* [16]	64×64	76.7	71.1	23.3	28.9	74.5
	128×128	79.3	80.5	20.7	19.5	80.3
	256×256	79.1	77.2	20.9	22.8	78.4
Su *et al.* [18]	64×64	71.1	69.5	28.9	30.5	70.4
	128×128	72.2	71.8	27.8	28.2	72.6
	256×256	76.6	80.7	23.4	19.3	78.0
Aizenburg *et al.* [19]	64×64	32.3	44.2	67.7	55.8	40.6
	128×128	75.8	71.4	24.2	28.8	74.3
	256×256	85.3	80.5	24.7	19.5	83.7
Proposed Method	64×64	91.5	88.7	8.5	11.3	90.2
	128×128	94.3	89.3	5.7	10.7	92.5
	256×256	97.9	92.4	2.1	7.6	95.4

increased, the results show that our method outperforms the results of prior works for all block sizes.

Next, we analyze our proposed method for image splicing detection. We consider the scenario that the original image and the spliced region have different blur types. For instance, original image has motion blur due to hand shake or camera motion while the spliced region has out-of-focus blur. We set up a dataset of tampered images exhibiting blur type inconsistency by replacing the central region of 200 out-of-focus blurred images with motion blurred regions and the central region of 200 out-of-focus blurred images with motion blurred regions. The size of tampered region is 128×128 and 256×256. To measure the performance, the ground truth of the blur types are used. Since some of the images may have sharp regions, we use the method in [27] in advance to discriminate blur/sharp areas. We define two classes including tampered region as positive class and authentic region as negative class. Table 2 shows the performance of our method for tampered region detection with size of 128×128 and 256×256.

Fig. 3 (a) shows an authentic motion blur image and Fig. 3 (b) is a tampered image generated by splicing an out-of-focus blurred region into the image (a). Fig. 3 (c) and (d) shows the discrimination results of the image (a) and (b) into three regions after local blur kernel estimation and clustering. After final blur type classification of the regions, the blur type of three regions in (c) is detected as motion blur. This reveals that there is no inconsistency in the blur types. The regions in (d) have different blur types including motion and out-of-focus blur. The region in the top left corner has out-of-focus blur while the other two regions have motion blur. This is an inconsistency in the blur type of the image because there is no motion object in the image and all regions should have the same blur type. This inconsistency in the blur type of the regions is an evidence of image tampering.

3.1. Cluster Number Selection

We study on the effect of number of clusters on the accuracy of tampered region detection. Consider an image with partial out-of-focus and motion blur types. If we select two clusters ($s = 2$), the image blocks are categorized into two regions with out-of-focus and motion blur types. By increasing the number clusters ($s > 2$), the image blocks are categorized not only based on the blur type but also based on the blur degree and the image content. For example, if two regions in the image have different motion directions, the motion blurred blocks are categorized into different clusters. However, since in the last part of our proposed approach we estimate the blur kernels of the regions, the kernels estimated from the regions are classified into out-of-focus or motion blur types.

Table 2. Tampering detection performance of our method

Tampered Region Size	TPR (%)	TNR (%)	Type I Error (%)	Type II Error (%)	Accuracy (%)
128×128	83.0	85.5	17.0	14.4	85.4
256×256	88.0	94.5	12.0	5.4	93.6

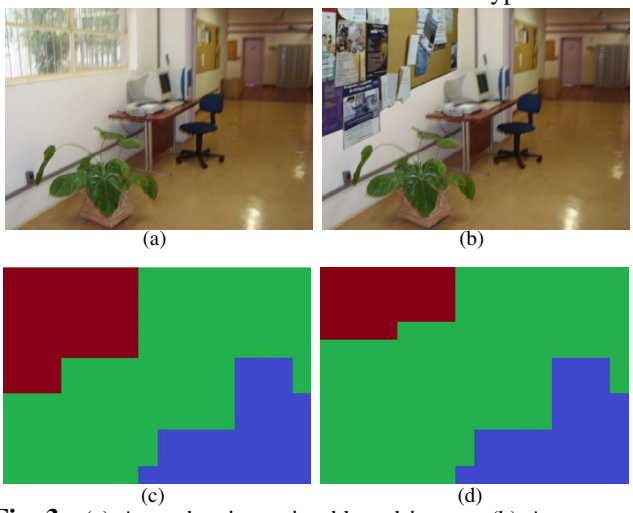

Fig. 3. (a) An authentic motion blurred image. (b) A tampered image generated by splicing an out-of-focus blurred region into the image (a). (c) and (d) show three regions as the result of clustering of the images (a) and (b), respectively.

4. CONCLUSION

A novel method for image tampering detection was proposed based on partial blur detection and classification. The input image was partitioned into blocks and the prior models of the image blocks were predicted to use in the local blur kernel estimation. Then, the local blur kernels of image blocks were estimated and a clustering method was used to categorize the image blocks with similar blur kernels into different regions. Finally, the blur kernels of the clusters were estimated and the clusters were classified into the different blur types. The experimental results showed that the proposed method could be used successfully for image splicing detection. In the current work we assumed simple form of blur kernels including uniform motion blur and symmetric out-of-focus blur which is correct for most cases. However, for some cases the blur kernel may have complex forms. In the future, more complicated forms of blur kernels, blur kernel analysis and blur kernel accuracy measurement will be done to improve the result of tampering detection.

5. REFERENCES

[1] H. Farid, "Image Forgery Detection," *IEEE Signal Processing Magazine*, 26(2), pp. 16-25, 2009.

[2] C. Popescu and H. Farid, "Exposing Digital Forgeries by Detecting Traces of Resampling," *IEEE Trans. Signal Processing*, vol. 53, no. 2, pp. 758-767, 2005.

[3] M. C. Stamm, and K. J. R. Liu, "Forensic Detection of Image Manipulation Using Statistical Intrinsic Fingerprints," *IEEE Trans. Inf. Forensics Security*, vol. 5, no. 3, pp. 492-506, 2010.

[4] T. Bianchi and A. Piva, "Image Forgery Localization via Block-Grained Analysis of JPEG Artifacts," *IEEE Trans. Inf. Forensics Security*, vol. 7, no. 3, pp. 1003-1017, 2012.

[5] H. Cao and A. C. Kot, "Accurate Detection of Demosaicing Regularity for Digital Image Forensics," *IEEE Trans. Inf. Forensics Security*, vol. 4, no. 4, pp. 899-910, 2009.

[6] P. Ferrara, T Bianchi, A. D. Rosa and A. Piva, "Image Forgery Localization via Fine-Grained Analysis of CFA Artifacts," *IEEE Trans. Inf. Forensics Security*, vol. 7, no. 5, pp. 1566-1577, 2012.

[7] A. Swaminathan, M. Wu, and K. J. R. Liu, "Digital Image Frensics via Intrinsic Fingerprints," *IEEE Trans. Inf. Forensics Security*, vol. 3, no. 1, pp. 101-117, 2008.

[8] M. Chen, J. Fridrich, M. Goljan, and J. Lucas, "Determining Image Origin and Integrity Using Sensor Noise," *IEEE Trans. Inf. Forensics Security*, vol. 3, no. 1, pp. 74-89, 2008.

[9] M. K. Johnson and H. Farid, "Exposing Digital Forgeries in Complex Lighting Environments," *IEEE Trans. Inf. Forensics Security*, vol. 2, no.3, pp. 450-461, 2007.

[10] K. Bahrami, A. C. Kot, and J. Fan, "Splicing Detection in Out-of-Focus Blurred Images," in *Proc. WIFS*, pp. 144-149, 2013.

[11] Y. Sutcu, B. Coskun, H. T. Sencar, and N. Memon, "Tamper Detection Based on Regularity of Wavelet Transform Coefficients," in *Proc. ICIP*, pp. 397-400, 2007.

[12] J. Wang, G. Liu, B. Xu, H. Li, Y. Dai, and Z. Wang, "Image Forgery Forensics Based on Manual Blurred Edge Detection," in *Proc. Multimedia Information Networking and Security*, pp. 907-911, 2010.

[13] G. Cao, Y. Zhao, and R. Ni, "Edge-based Blur Metric for Tamper Detection," *Journal of Information Hiding and Multimedia Signal Processing*, vol. 1, no. 1, pp. 20-27, 2010.

[14] X. Wang, B. Xuan, and S. Peng, "Digital image forgery detection based on the consistency of defocus blur," in *Proc. Intelligent Information Hiding and Multimedia Signal Processing*, pp. 192-195, 2008.

[15] P. Kakar, N. Sudha, and W. Ser, "Exposing Digital Image Forgeries by Detecting Discrepancies in Motion Blur," *IEEE Trans. on Multimedia*, vol. 13, no. 3, pp. 443-452, 2011.

[16] X. Chen, J. Yang, Q. Wu, J. Zhao, and X. He, "Directional high-pass filter for blurry image analysis," *Signal Processing:Image Communication*, vol. 27, pp. 760-771, 2012.

[17] R. Liu, Z. Li, and J. Jia, "Image partial blur detection and classification," in *Proc. CVPR*, pp. 1-8, 2008.

[18] B. Su, S. Lu, and C. L. Tan, "Blurred Image Region Detection and Classification," in *ACM Multimedia*, pp. 1397-1400, 2011.

[19] I. Aizenberg, D. V. Paliy, J. M. Zurada, and J. T. Astola, "Blur Identification by Multilayer Neural Network Based on Multivalued Neurons," *IEEE Trans. on Neural Network*, vol. 19, no. 5, pp. 883-898, 2008.

[20] A. Levin, Y. Weiss, F. Durand, and W. T. Freeman, "Efficient Marginal Likelihood Optimization in Blind Deconvolution," in *Proc. CVPR*, pp. 2657-2664, 2011.

[21] L. Yuan, J. Sun, L. Quan, H. Y. Shum, "Blurred/Non-Blurred Image Alignment using Sparseness Prior," in *Proc. ICCV*, 2007.

[22] R. Fergus, B. Singh, A. Hertzmann, S. T. Roweis, W. T. Freeman, "Removing Camera Shake from a Single Photograph," *ACM Trans. Graph.*, vol. 25, no. 3, pp. 787-794, 2006.

[23] A. Mittal, A. Moorthy, and A. Bovik, "No-reference image quality assessment in the spatial domain," *IEEE Trans. on Image Processing*, vol. 21, no. 12, pp. 4695-4708, 2012.

[24] S. Cho and S. Lee, "Fast motion deblurring," *ACM Trans. Graph.*, vol. 28, no. 5, 2009.

[25] Z. Hu and M. H. Yang, "Good Regions to Deblur," in *Proc. ECCV*, 2012.

[26] http://www.flicker.com

[27] K. Bahrami, A. C. Kot, and J. Fan, "A Novel Approach for Partial Blur Detection and Segmentation," in *Proc. ICME*, pp. 1-6, 2013.